Energy-Dependent Three-Body Loss in 1D Bose Gases

Laura A. Zundel, Joshua M. Wilson, Neel Malvania, Lin Xia, Jean-Felix Riou, and David S. Weiss

Phys. Rev. Lett. **122**, 013402 — Published 9 January 2019

DOI: 10.1103/PhysRevLett.122.013402

Energy-dependent 3-body loss in 1D Bose gases

Laura A. Zundel, Joshua M. Wilson, Neel Malvania,
Lin Xia,* Jean-Felix Riou, and David S. Weiss†
Physics Department, The Pennsylvania State University,
104 Davey Lab, University Park, PA 16802

(Dated: December 12, 2018)

Abstract

We study the loss of atoms in quantum Newton's cradles (QNCs) with a range of average energies and transverse confinements. We find that the three-body collision rate in one-dimension is strongly energy dependent, as predicted by a strictly 1D theory. We adapt the theory to atoms in waveguides, then using detailed momentum measurements to infer all the collisions that occur, we compare the observed loss to the adapted theory and find that they agree well.

PACS numbers: 34.50.Cx, 34.10Jk, 34.90.+q

* Present address: Beijing National Laboratory for Condensed Matter Physics, Institute of Physics, Chinese Academy of Sciences, Beijing 100190, China
† email: dsweiss@phys.psu.edu

When three ultracold atoms exit a collision as a molecule and an atom, both particles escape typical atom traps. While these inelastic 3-body collisions are often an atomic density limiting nuisance [1], they can sometimes be usefully employed. They enable the observation of Efimov trimer states [2, 3], they allow detection of triply occupied states in optical lattices [4], they can cool 1D gases [5, 6], and they can probe local three body correlation functions in 3D [7] and 1D Bose gas experiments [8–10]. When the two-body scattering length exceeds other length scales, as it often does, 3-body inelastic collisions exhibit analytically calculable universal behavior [11–13]. The collision rate in 3D is energy-independent [14], but a steep energy dependence has been predicted in 1D [13].

In 3D, inelastic 3-body collision rates have been measured in both thermal and quantum degenerate gases [7], but in 1D they have only been measured in the latter [8, 9] because one needs to reach very low temperatures to satisfy the quasi-1D requirement of being only in the ground state of a waveguide [15]. By making a QNC excitation [16], which we explain below, we give our 1D gases kinetic energies that exceed the quantum degeneracy energy scale. After the initial oscillations dephase, the atoms' axial motion can be well described semiclassically, so 3-body inelastic collisions involve distinct particles, rather than emerging from overlapping, correlated wavefunctions. Thus, independent of the many-body physics that dominates quantum degenerate gases, we can study the 3-body loss constant itself, K_3^{1D}, observing its strong dependence on center of mass collision energy, E_{cm} [13]. Our results are not inconsistent with a predicted sixth order dependence on the 1D scattering length, a_{1D}, although, as we will show, our experiment is rather insensitive to this dependence.

We begin our experiments with a BEC of $\sim 5 \times 10^5$ ^{87}Rb atoms in the $|F = 1, m_F = 1\rangle$ state. A 2D blue-detuned optical lattice with wavevector $k = 2\pi/772$ nm is ramped up to a lattice depth $V_0 = 40E_R$ in 23 ms, where the recoil energy $E_R = (\hbar k)^2/2m$ and m is the mass of ^{87}Rb. We thus create an array of ~ 3500 tubes with minimal tunneling between tubes. After loading the atoms into the 2D lattice, the atom number is 4.9×10^5 and the transverse Thomas-Fermi radius of the cloud is $R_{TF} = 13.0$ μm. We also create somewhat lower density distributions by lengthening the ramp up time to 70 ms, resulting in a distribution with $R_{TF} = 13.9$ μm and 4.5×10^5 atoms. Axial confinement is provided by a red-detuned optical dipole trap of depth $U_o = 10E_R$, chosen to be less than half the energy splitting between the transverse ground and second excited states. This condition ensures that even the most highly axially excited atoms do not have enough energy to excite to higher transverse states via binary collisions. Also, most

atoms that are transversely excited due to spontaneous emission are lost when they collide among themselves and vibrationally de-excite [15].

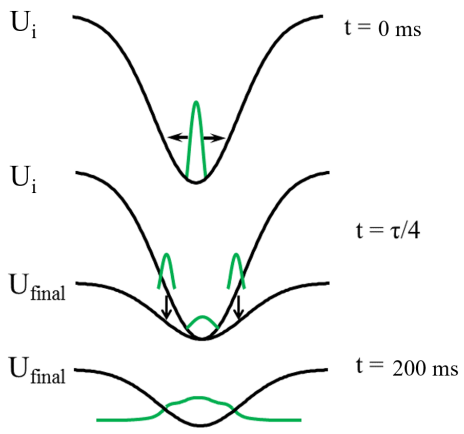

FIG. 1: (Color Online) Axial trap sequence used to change the average energy of the atoms. At $t = 0$ ms most of the atoms are diffracted and the axial trap depth is immediately increased from U_o to U_i. When the atoms reach their turning point a quarter-cycle later the axial trap is decreased to $U_{final} = \{9.3, 10, 11, 12\}E_R$ for $V_{latt} = \{36, 40, 45, 50\}E_R$ respectively. The atoms then evolve for 200 ms, by which time the distributions are fully dephased.

We take the 1D gases out of equilibrium by setting up QNCs [16] of varying average energy, $\overline{E_o}$. The QNC is started by applying a sequence of two standing wave pulses along the axis of the tubes, made from beams with wavenumber $\sim k$ and intensity 18 W/cm^2 [17]. Each pulse is 23 μs long and there is a 33 μs pause between pulses. Most atoms end up in a superposition of $\pm 2\hbar k$ momentum states, although due to interactions $\sim 30\%$ of the atoms remain near zero momentum. Immediately after diffraction, the lattice and axial depths are suddenly ramped to V_{latt} and U_i respectively, where V_{latt} ranges from $36E_R$ to $50E_R$. The atoms are allowed to expand in the deeper trap for a quarter of the oscillation period of U_i (see Fig.1). At their turning point, we remove part of their mechanical energy by suddenly decreasing the axial depth to U_{final}, which is chosen to be less than half the energy splitting between the transverse ground and second excited states of the corresponding V_{latt}. We then wait for approximately 20τ, where $\tau = 10$ ms is the typical axial oscillation period in the final trap. During this time in the Gaussian, and thus

significantly anharmonic axial trap, the atoms' motion dephases within each tube and the density distribution ceases to change on the τ timescale. We continue to let the atoms evolve for a time t_{ev}. At t_{ev} we turn off the dipole trap and adiabatically ramp down the lattice to $2.5E_R$ in 0.14 ms in order to remove most of the transverse trapping energy and residual atom interaction energy. We then suddenly complete the turn-off of the lattice light and let the atoms expand for 15 ms time-of-flight.

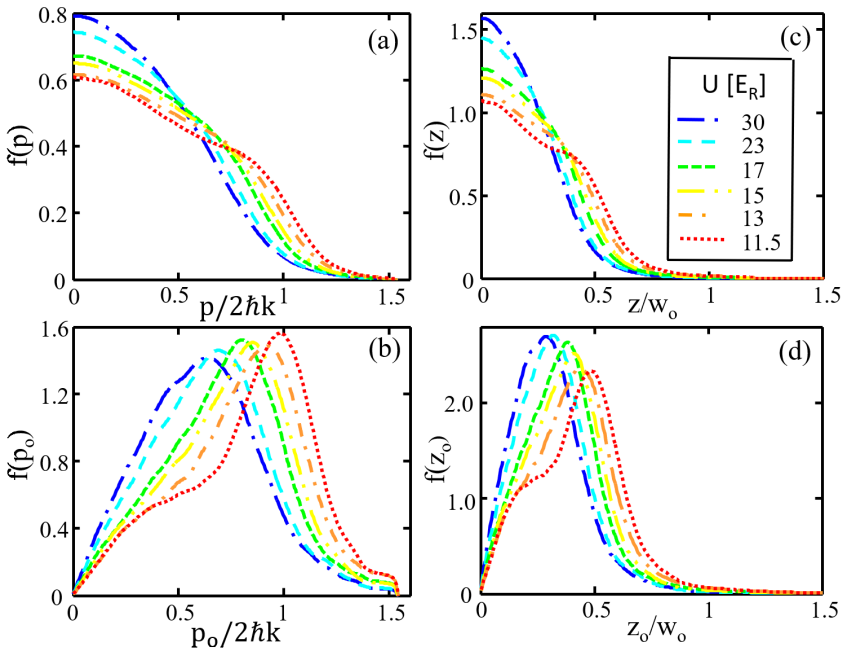

FIG. 2: (Color Online) Normalized 1D trap distributions, for various QNC energies and a $45E_R$ lattice confinement. (a) $f(p)$. (b) $f(p_o)$. (c) $f(z)$. (d) $f(z_o)$. The curves for $f(p)$ and $f(z)$ are normalized to 0.5, while the $f(p_o)$ and $f(z_o)$ distributions are normalized to 1. In (c) and (d) $w_0 = 42.6$ μm is the beam waist of the axial dipole trap.

We take an absorption image at each t_{ev}, integrating transversely to get the axial momentum distribution, $f(p)$, and integrating the whole image to find the total atom number. The initial $f(p)$ for various $\overline{E_o}$ are shown in Fig. 2a. Because the atoms have more than 20 times as much mechanical energy as interaction energy, their motion can be well described semi-classically [15]. Since loss depends on the axial spatial distribution, $f(z)$, and the collision energy of the particles, we derive both $f(z)$ and the distribution of peak momenta, $f(p_o)$, from $f(p)$ via energy conservation as follows. The mechanical energy of each atom is $E_o = p_o^2/2m = p^2/2m + U(z)$, where p_o is the amplitude of the atom's momentum oscillation and $U(z)$, a Gaussian function, is the potential

energy at the axial position z. We extract from $f(p)$ the distribution of peak momenta $f(p_o)$ using the relation $f(p) = \int_0^{p_o} G(p, p_o) f(p_o) dp_o$, where $G(p, p_o)$ is the probability that an atom with momentum amplitude p_o has momentum p [15]; the results are shown in Fig. 2b. To derive $f(z)$, we use conservation of energy to convert $f(p_o)$ to $f(z_o)$, the axial spatial amplitude distribution (Fig. 2d). Then, using a procedure like the inverse of the transformation from $f(p_o)$ to $f(p)$, we calculate $f(z)$ from $f(z_o)$; it is plotted in Fig. 2c.

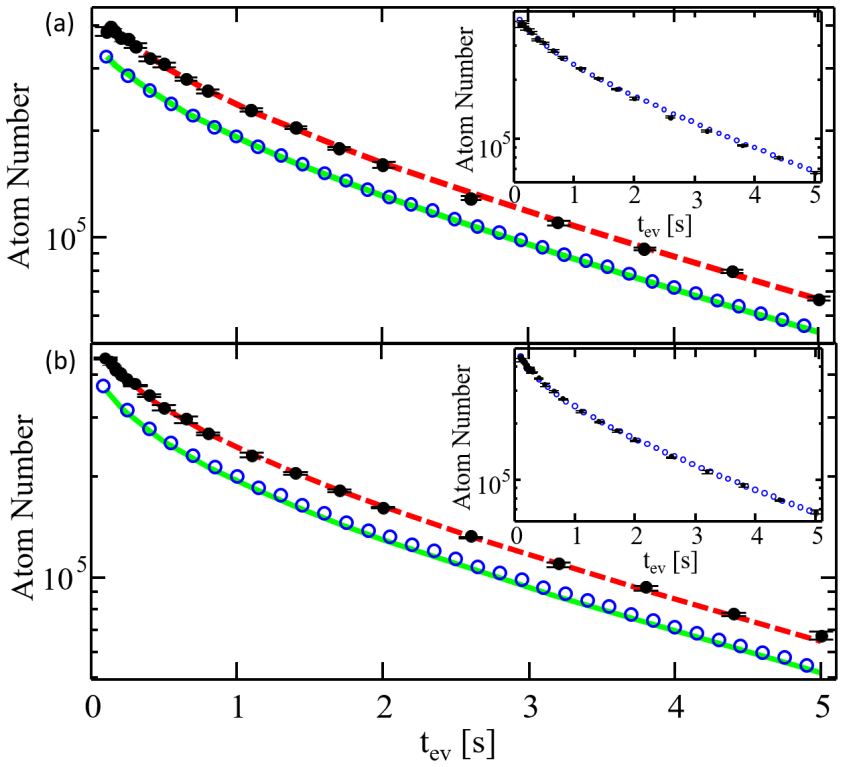

FIG. 3: (Color Online) Total atom number as a function of holding time in a (a) lower and (b) higher density QNC distribution with $\overline{E}_o = 3.05 E_R$ in a $50 E_R$ lattice depth. Black circles are the average of six data points; the standard deviation of these points are smaller than the marker size. The red dashed lines are the fits of the experimental data curves to Eq. 1. The insets show the direct comparison between the experimental data curves and the theoretical curves (open blue circles) derived from the global fit of the loss model (Eq. 3) to the data. In order to make many such comparisons on the same plot (see Fig. 4), we fit the theoretical curves to Eq. 1 (solid green lines in the main figures). To make solid green curves and blue circles more visible, they have been offset by a factor of 0.8. As is clear from the insets, without the offset they would be nearly overlapped.

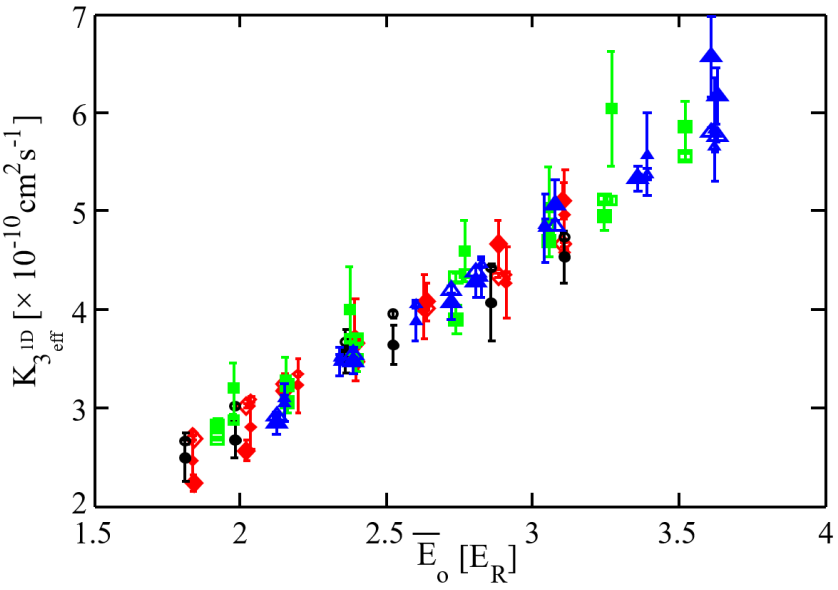

FIG. 4: (Color Online) Experimental and theoretical $K_{3_{eff}}^{1D}$. The experimental points are the solid symbols (larger for higher density and smaller for lower density) shown as red diamonds, black circles, green squares, and blue triangles for 36, 40, 45, and $50E_R$ lattice depths respectively. We obtain the experimental points by fitting the experimental loss curves to Eq. 1. $K_{3_{eff}}^{1D}$ increases with energy at all lattice depths, but does not depend on the lattice depth. We obtain the theoretical points (hollow symbols) by fitting the decay curves derived from our detailed loss model (Eq. 3) to Eq. 1.

We measure loss curves like those shown by the black circles in Fig. 3 for each initial $\overline{E_o}$. As a first step in our analysis, we simply fit each curve to find an effective 3-body loss coefficient, $K_{3_{eff}}^{1D}$. This ignores the details of $f(p_o)$ and $K_3^{1D}(E_{cm})$, but allows us to compare all the decay curves in one figure. Specifically, we fit each decay curve to:

$$\frac{dN_{\text{tube}}}{dt} = -K_1 N_{\text{tube}} - K_{3_{eff}}^{1D} N_{\text{tube}}^3 \int f(z)^3 dz \tag{1}$$

where $N_{\text{tube}} = 5N_o\pi/2k^2R_{TF}^2[1-(x/R_{TF})^2-(y/R_{TF})^2]$ is the atom number in a tube at position (x,y). To calculate the total loss we sum over all tubes. The fit parameters are $K_{3_{eff}}^{1D}$, K_1 and the initial atom number, N_o. K_1 is mostly due to lattice spontaneous emission, and it depends on V_{latt} and U_{final}, so we constrain all curves with the same V_{latt} and U_{final} to have the same K_1 [15]. The fits are shown by the red dashed lines in Fig. 3. We plot $K_{3_{eff}}^{1D}$ as a function of $\overline{E_o}$, shown in Fig. 4 by the solid red diamonds, black circles, green squares, and blue triangles corresponding

to $V_{latt} = 36$, 40, 45, and $50E_R$. The larger and smaller symbols correspond to higher and lower density distributions respectively. If the collisions were energy-independent, the plot would be a horizontal line. Instead, the data shows that distributions with higher $\overline{E_o}$ have a higher $K_{3_{eff}}^{1D}$. The strong energy dependence we measure arises even though there is considerable averaging inherent to the broad $f(p)$ distributions in a QNC. The data in Fig. 4 also shows that the loss is independent of lattice depth, in apparent contradiction of the 1D semi-classical model.

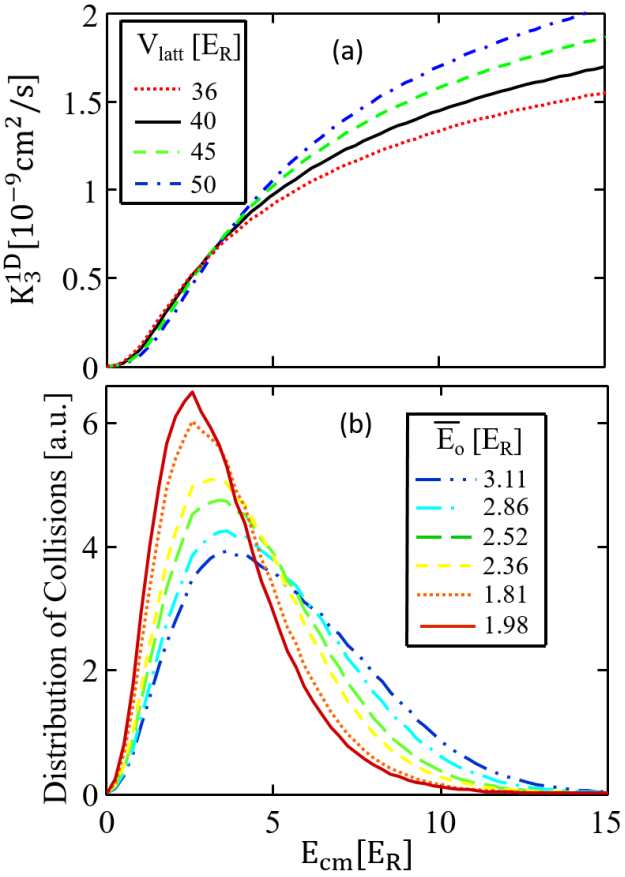

FIG. 5: (Color Online) (a) Plot of K_3^{1D} as a function of the center of mass collision energy for atoms in a 36, 40, 45, and $50E_R$ lattice. Note that, although K_3 is constant, deeper lattices have higher $K_{3_{max}}^{1D}$. (b) Plot of the distribution of collisions in the $40E_R$ lattice as a function of the collision energy for different $\overline{E_o}$.

The semi-classical motion limit in 1D gives us such detailed knowledge of all aspects of the particles' motion that we can keep track of all collisions and their E_{cm}, while also taking into account the p_o distributions and the way they evolve due to heating [15]. We can use this knowledge

to test whether a given $K_3^{1D}(E_{cm})$ is consistent with our decay data. To model the energy dependence of loss in a QNC, we start with the strictly 1D semi-classical model of three-body collisions [13] which gives $K_3^{1D} = Ca_{1D}^6 E_{cm}^3$, where K_3^{1D} is the three-body collision cross section in 1D and C is a proportionality constant that depends on the atom. The basic adaptation of 1D theory to atoms in a waveguide has long been known, $a_{1D} \approx -2a_\perp^2/a_{3D}$ [18]. Since we expect loss to only be suppressed in 1D compared to 3D, not enhanced, we expect the loss rate at high E_{cm} to saturate at the thermal 3D loss rate, $6 \times K_3$, where K_3 is the three-body collision cross section in a 3D quantum degenerate gas [7]. We therefore introduce E_l, a collision energy to characterize this saturation. Since the transverse vibrational excitation energy is characteristic of the crossover to the 3D, we assume that E_l scales with it, i.e., $E_l = 2C_2\hbar^2/ma_\perp^2$, where C_2 is a constant to be empirically determined. Perhaps the simplest function that smoothly meets our criteria at low and high energies with a variable crossover energy is:

$$K_3^{1D}(E_{cm}) = C' a_\perp^{12} E_{cm}^3 \left(\frac{C' a_\perp^{12} E_{cm}^3}{K_{3_{max}}^{1D}(\frac{E_{cm}}{E_{cm}+E_l})} + 1 \right)^{-1} \tag{2}$$

where $K_{3_{max}}^{1D} = 6 \times K_3/3\pi^2 a_\perp^4$ [8]. We have also tried other ways to roll off K_3^{1D} at high energy, and we find that the fit quality is not very sensitive to the form of the roll off *. Note that there is not enough energy in a 3-body collision to transversely excite an atom until $E_{cm} > 20\ E_R$. So even as K_3^{1D} saturates, the dynamics are one dimensional until a 3-body inelastic collision occurs.

We calculate the loss rate for all possible collisions by first discretizing the $f(z_o)$ distribution. We convert each $f(z_o)$ segment into corresponding spatial distributions, $f(z, z_o)$, then divide the total spatial distribution $f(z) = \sum_{z_o} f(z, z_o)$ into small segments of width Δz. The momentum of each atom within a Δz segment can be calculated from z and z_o. These momenta are then used to calculate E_{cm} for all momentum combinations, including all direction combinations. From the E_{cm}'s we use Eq. 2 to calculate the corresponding K_3^{1D}'s, which are then used to calculate the three body loss within each Δz. This loss is given by

$$\frac{dN_{\text{tube}}}{dt} = -K_1 N_{\text{tube}} - N_{\text{tube}}^3 \sum_{z_{o_i}=z_{o_1}}^{z_{o_f}} \sum_{z_{o_j}=z_{o_i}}^{z_{o_f}} \sum_{z_{o_k}=z_{o_j}}^{z_{o_f}} K_3^{1D}(E_{cm}) \int_z^{z+\Delta z} f(z', z_{o_i}, t) f(z', z_{o_j}, t) f(z', z_{o_k}, t) dz' \tag{3}$$

The lowest energy z_o group is z_{o_1} and the highest is z_{o_f}. To account for all collisions in Δz without double counting, collisions of particles with z_{o_i}, z_{o_j} and z_{o_k} are weighted by their relative probability. We use the measured $f(z)$ distributions as time evolves.

*See Supplemental Material for more information on the sensitivity to the roll off.

We use the K_1's and N_o's obtained from the fit to Eq. 1 to globally fit Eq. 3 to all of the loss data curves with C' and C_2 as free parameters, while K_3 is fixed to the weighted average of previous measurements [7, 8], $K_3 = 7.1 \times 10^{-30}$ cm^6/s. Because the fit quality is sensitive to the ratio of cloud sizes for the higher and lower densities, we fit using the measured size of the lower density cloud and allow the higher density cloud size to be a free parameter, restricting its value to be within its measurement uncertainty. We obtain the fit parameters $C' = 4.2(+0.18/-0.16) \times 10^{142}$ cm^{-10}J^{-3}s^{-1} and $C_2 = 28(+1.6/-3.1) \times 10^{-2}$. The bounds on the fit parameters are set by the uncertainty in the lower density cloud size. The blue circles in Fig. 3 show examples of the theoretical curves generated by this elaborate fit based on keeping track of all 3-body collisions.

Figure 5a shows $K_3^{1D}(E_{cm})$ at all lattice depths using these fit parameters. Fig. 5b shows the distribution of inelastic collisions as a function of E_{cm} for various values of $\overline{E_o}$ in a $40E_R$ lattice. We calculate this distribution by summing together the collisions that enter into Eq. 3 and sorting them by E_{cm}. The red dotted $36E_R$ line in Fig. 5a has a somewhat higher K_3^{1D} for $E_{cm} < 4E_R$ where there are many collisions, while the blue dash-dotted $50E_R$ line has a much higher K_3^{1D} for $E_{cm} > 4E_R$ where there are fewer collisions. The net effect is very weak dependence on lattice depth.

It is hard to visualize how the model fits the data by directly comparing the many theoretical curves to their corresponding experimental data curves (insets in Fig. 3). Instead, we fit each of the theoretical curves (like the blue circles in Fig. 3) to Eq. 1, using $K_{3_{eff}}^{1D}$ as a free parameter just as we did for the experimental data curves. These fits are shown by the green lines in Fig. 3. The $K_{3_{eff}}^{1D}$'s obtained by fitting the theoretical curves derived from the model (hollow symbols in Fig. 4) can then be compared to the $K_{3_{eff}}^{1D}$'s obtained by fitting the experimental loss (solid symbols in Fig. 4). The reduced chi-square value between the $K_{3_{eff}}^{1D}$'s for the theory and the data is 2.08. The model, defined in Eq. 2 and implemented with Eq. 3, captures the observed increase in $K_{3_{eff}}^{1D}$ with energy at all V_{latt}, and the approximate independence of $K_{3_{eff}}^{1D}$ on V_{latt}.

Studies of low temperature 1D gases have used a rather orthogonal way to look at 3-body loss, based on local correlations, $g_3(0)$ [8, 9]. As far as we know, the relationship between loss suppression in 1D by reduced $g_3(0)$ and by energy dependent K_3^{1D} has not been explored theoretically. The latter cannot readily be applied in equilibrium, where there is no possible semi-classical approximation. The former is problematic for a QNC where the system is not in thermal equilibrium and correlations must change dynamically as the atoms move [19]. Applying both approaches at the same time would constitute double counting that is inconsistent with observations. Loss sup-

pression by reduced $g_3(0)$ and energy dependent K_3^{1D} may be complementary ways of describing much of the same physics. More theory is needed.

In conclusion, we have measured the three-body loss rates in out-of-equilibrium 1D Bose gases with different average energies and transverse confinements. We find that they strongly depend on the energy of the colliding atoms, as a purely 1D theory predicts [13]. Still, a rigorous theory of 3-body inelastic collisions in waveguides is needed. Besides testing such a theory, our results will be important in studies of thermalization in out-of-equilibrium 1D gases [16, 20].

ACKNOWLEDGEMENTS

This works was supported by the Army Research Office Grant No. W911NF-16-1-0031 and NSF Grant No. PHYS-1707576.

[1] D. Lobser, A. Barentine, E. Cornell, and H. Lewandowski, Nature Physics **11**, 1009 (2015).

[2] J. Huckans, J. Williams, E. Hazlett, R. Stites, and K. OHara, Phys. Rev. Lett. **102**, 165302 (2009).

[3] T. B. Ottenstein, T. Lompe, M. Kohnen, A. Wenz, and S. Jochim, Phys. Rev. Lett. **101**, 203202 (2008).

[4] L. Xia, L. A. Zundel, J. Carrasquilla, A. Reinhard, J. M. Wilson, M. Rigol, and D. S. Weiss, Nature Physics **11**, 316 (2015).

[5] N. Syassen, D. M. Bauer, M. Lettner, T. Volz, D. Dietze, J. J. Garcia-Ripoll, J. I. Cirac, G. Rempe, and S. Dürr, Science **320**, 1329 (2008).

[6] M. Schemmer and I. Bouchoule, arXiv preprint arXiv:1806.09940 (2018).

[7] E. Burt, R. Ghrist, C. Myatt, M. Holland, E. Cornell, and C. Wieman, Phys. Rev. Lett. **79**, 337 (1997).

[8] B. L. Tolra, K. Ohara, J. Huckans, W. Phillips, S. Rolston, and J. Porto, Phys. Rev. Lett. **92**, 190401 (2004).

[9] E. Haller, M. Rabie, M. J. Mark, J. G. Danzl, R. Hart, K. Lauber, G. Pupillo, and H.-C. Nägerl, Phys. Rev. Lett. **107**, 230404 (2011).

[10] G. Smirne, R. Godun, D. Cassettari, V. Boyer, C. Foot, T. Volz, N. Syassen, S. Dürr, G. Rempe, M. Lee, *et al.*, Phys. Rev. A **75**, 020702 (2007).

[11] B. Esry, C. H. Greene, and J. P. Burke Jr, Phys. Rev. Lett. **83**, 1751 (1999).

[12] C. H. Greene, B. Esry, and H. Suno, Phys. Rev. A **737**, 119 (2004).

[13] N. P. Mehta, B. Esry, and C. H. Greene, Phys. Rev. A **76**, 022711 (2007).

[14] J. P. DIncao, H. Suno, and B. D. Esry, Phys. Rev. Lett. **93**, 123201 (2004).

[15] J.-F. Riou, L. A. Zundel, A. Reinhard, and D. S. Weiss, Phys. Rev. A **90**, 033401 (2014).

[16] T. Kinoshita, T. Wenger, and D. S. Weiss, Nature **440**, 900 (2006).

[17] S. Wu, Y.-J. Wang, Q. Diot, and M. Prentiss, Phys. Rev. A **71**, 043602 (2005).

[18] M. Olshanii, Phys. Rev. Lett. **81**, 938 (1998).

[19] K. Kheruntsyan, D. Gangardt, P. Drummond, and G. Shlyapnikov, Phys. Rev. Lett. **91**, 040403 (2003).

[20] M. Gring, M. Kuhnert, T. Langen, T. Kitagawa, B. Rauer, M. Schreitl, I. Mazets, D. A. Smith, E. Demler, and J. Schmiedmayer, Science **337**, 1318 (2012).